JOINT INSTITUTE FOR NUCLEAR RESEARCH

Veksler and Baldin Laboratory of High Energy Physics

FINAL REPORT ON THE SUMMER STUDENT PROGRAM

Acquaintance with spectrometric equipment for nuclear experiments

Supervisor:

Sergey Tyutyunnikov,

doctor of science

Student:

Polina Sushkova, Russia

Kazan Federal University

Participation period:

July 01 – August 10

Dubna 2019

1. Optical spectrometry of impurities

Abstract

Threaded HF discharge for analysis of the atomic composition of human hair is used. A special technique of samples ashing for further researches is mastered. The emission spectrum of the hair is obtained. The analysis of obtained spectrum shows the presence of elements such as Ca and Mn.

Introduction

There is a rapid growth in studying of microelements concentrations in human hair around the world. Information that provided by these researches can say a lot about metabolism of the person. Many elements such as selenium, zinc, copper and manganese are directly involved in metabolic processes. The usual analysis of blood shows content of microelements. Anyway, the maximal period that it covers is a few days before the blood test [1]. Analysis of hair can determine content of metals during the period of last 3-6 months. It is the most fast and effective way to obtain adequative information about deficiency or excess of elements in the organism [2].

One of the methods of studying the atomic composition of organic compounds in human hair is using a HF filamentary discharge [3]. It can be more simplified way in analysis of substances than the method of researches based on inductively coupled plasma [4].

Analysis of solids.

Previously, a special device that using capacitive HF discharge was proposed for the analysis of the atomic composition of solids [3]. To study the composition of organic substances with a temperature of heat resistance not more than 300 ºC it was developed a burner (Fig. 1.1). Temperature regulation in the sample cavity is carried out by changing the mass of the cylinder, its material and the depth of the cavity.

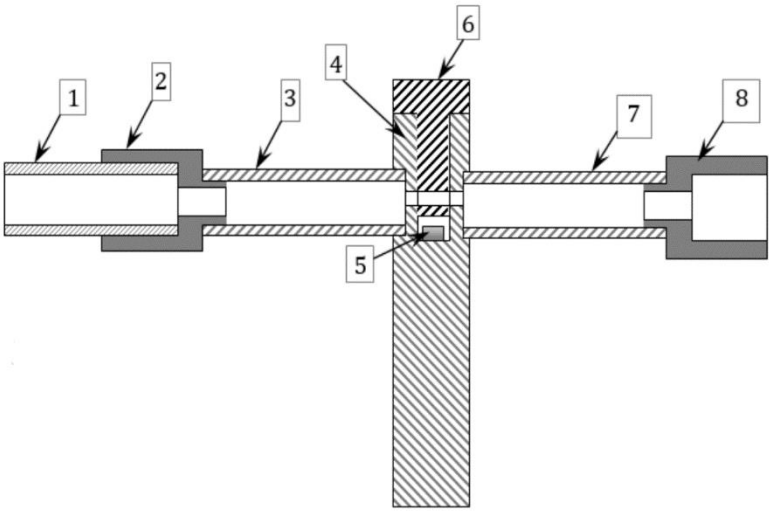

Figure 1.1. Burner for organic substances. 1 – inlet fitting, 2 – first cylindrical electrode, 3 – ceramic tube, 4 – metal cylinder, 5 – sample, 6 – cover, 7 – ceramic tube, 8 – additional electrode.

When HF voltage is applied, the discharge is initiated between the electrodes, the second electrode is heated rapidly, and the sample is melted and evaporated. Atoms of the sample material enter hot discharge plasma, collide with electrons and atoms of argon, and are repeatedly excited (ionized) with subsequent relaxation into the ground state [3]. The spectra of plasma radiation are analyzed by a spectrometer.

Sample 5 (Fig. 1.1) was inserted into the cylinder 4 and closed with a cover 6 stainless steel. Then the argon and the discharge were switched on. Within 5 minutes, the sample was heated in the atmosphere of argon. Then there was a melting and concentration of the sample with the emission of molecules of the sample into the discharge. In the experiments it was found that the bulk of the radiation spectra are molecules of organic components of the sample. The peaks of trace elements are very small.

Samples

Analysis of atomic composition of hair involves primary samples preparation. Firstly, samples have to pass the stage of ashing including the argon flow for 10 minutes. The resulting ash is crushed, then C_2H_5OH is added to this consistency. Secondly, these components are mixed, and after that, the resulting mixture is used in creating a thin film for further analysis.

There is an image of a visual comparison of the hair samples after samples preparation by our method and by conventional ashing (Fig. 1.2).

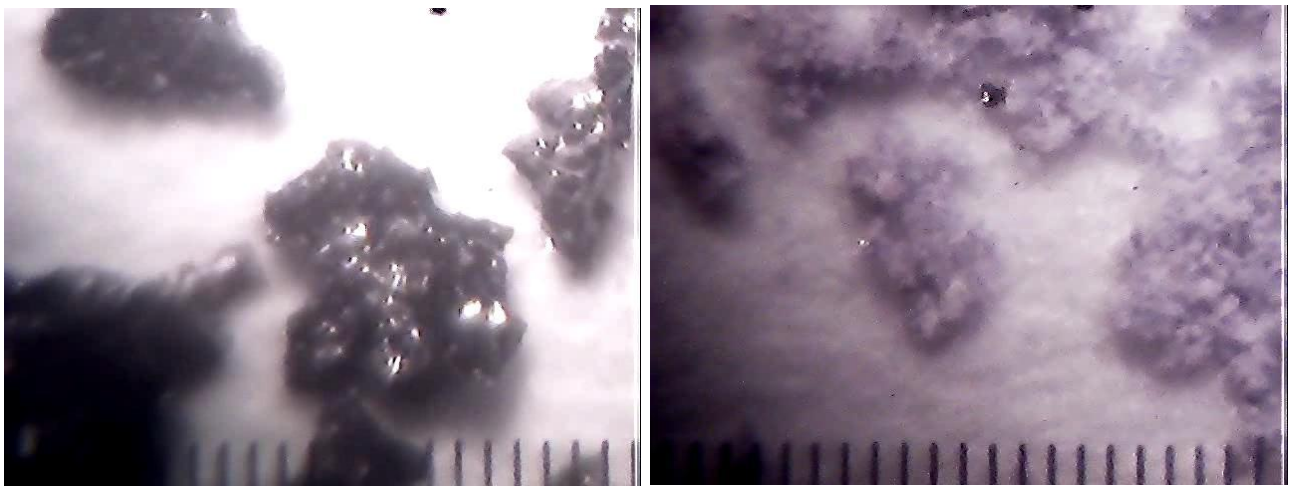

Figure 1.2. Photos of samples after 1 hour of preparation (left) and after ashing (right). The distance between the strokes – 100mkm.

Films of ashing samples are replaced on target which is lit by the light source. The source is a laser Cobolt 06-Tor with wavelength 1064 nm. The laser beam passes through the lens, hits the sample and vaporizes the substance particles into a quartz tube with argon.

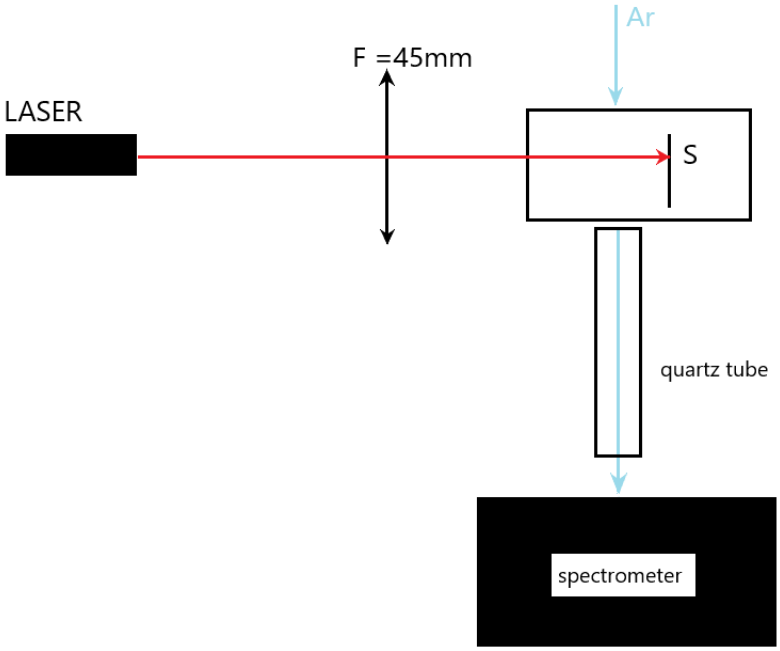

Figure 1.3. Scheme of experiment. Laser beam with wavelength 1064 nm passes through the lens with focal length 45 mm. S – sample of human hairs, Ar – argon.

Experimental results and discussions

During the experiment we have received spectrum of the atomic composition of hair samples. Figures 4 and 5 show a part of the emission spectrum where you can see distinctly wavelengths of Ca and Mn. There were used optical monochromator-spectrograph MS 520 by SOL instruments, Republic of Belarus.

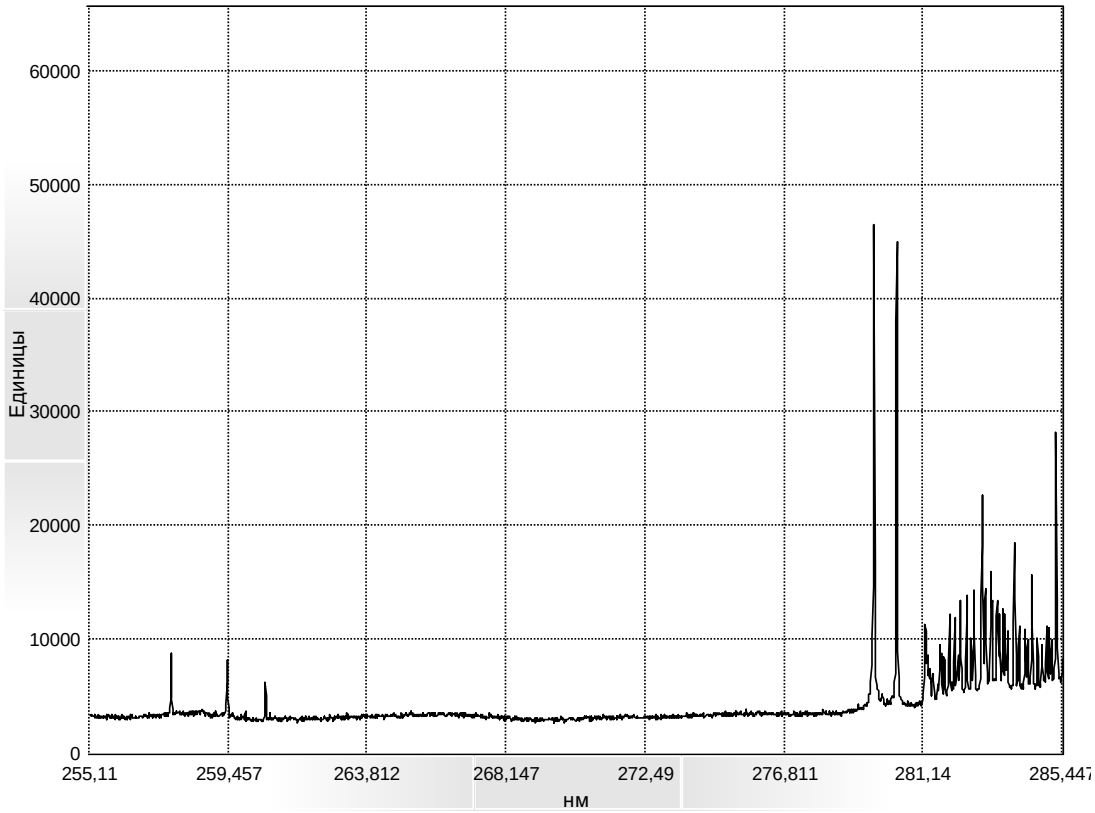

Figure 1.4. The emission spectrum of the hair. The horizontal axis is the wavelength in nanometers, the vertical is the amplitude of the signal in relative units. Wavelengths of Mn: 280,11 nm and 280,27 nm.

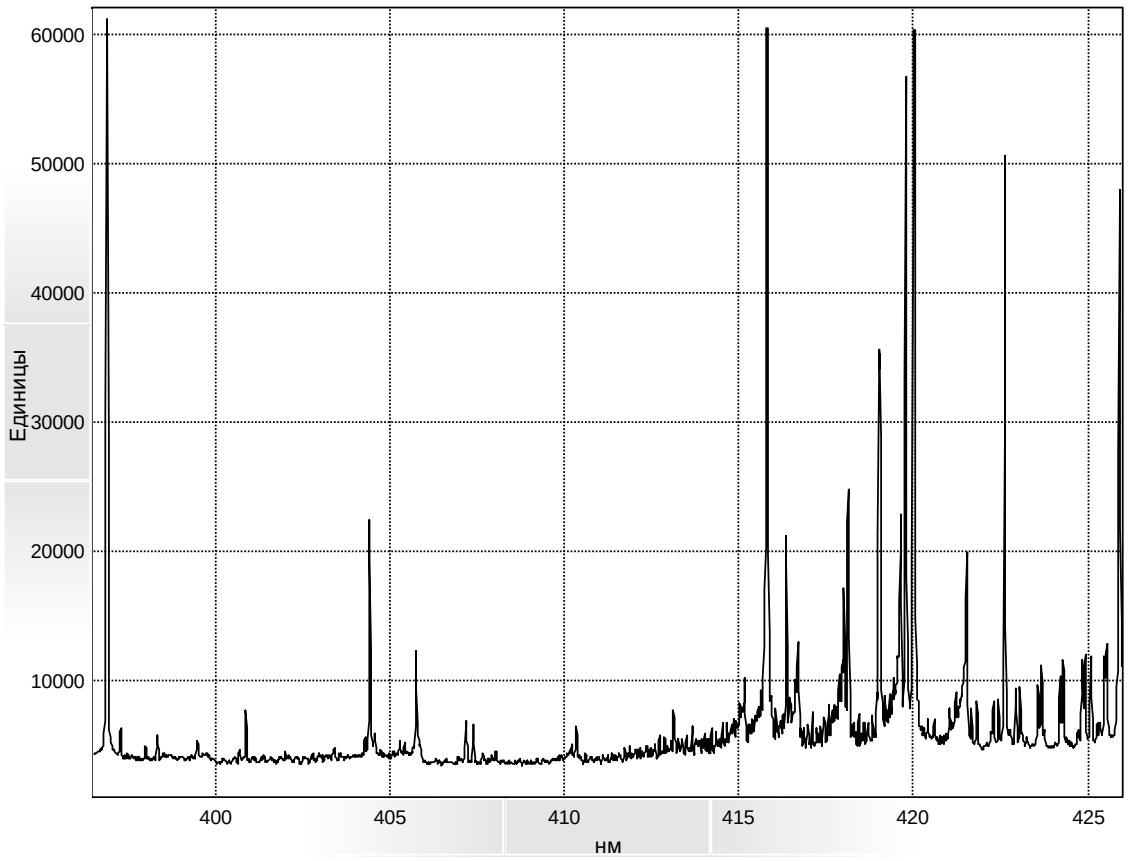

Figure 1.5. The emission spectrum of the hair. Wavelengths of Ca: 396,85 nm and 422,67 nm.

Conclusion

In this work, we have studied how to use HF filamentary discharge for analyzing the atomic composition of organic compounds in human hair. The complexity of the experiment was that samples have to pass necessary primer preparation. There was made special procedure for production of probe using methods of ashing it. Graphs of the emission spectrum were presented as results. Analysis of organic compounds in human hair shows contents of elements such as Ca and Mn. It means that possibility of using this technique for analyzing the atomic composition with enough sensibility is not inferior to the modern method of analysis.

2. Silicon detectors for radiation detection based on pixel structures

Abstract

The assembly of sixteen element matrix based on micropixel avalanche photodiodes of the type MAPD-3NM are presented. Measurements of the I-V characteristics were carried out, as a result of which the breakdown and operating voltages were determined. The photodiodes were selected with the same operating voltage for homogeneous assembly. The dark current and photocurrent of devices are measured.

Introduction

The rapid progress in the physics and technology of semiconductors in the last century led to the creation of solid-state analogs, almost all vacuum devices, except for photomultiplier tubes (PMT). Although, after the discovery at the beginning of the 50s of the last century, the photocurrent enhancement effect in silicon and germanium avalanche photodiodes [5,6] and the creation of the basic theory of impact ionization in semiconductors [7-12], certain prospects appeared, but to create adequate solid-state analogs of a photomultiplier required years of research. The avalanche photodiodes (APD) known at that time were significantly inferior to the photomultiplier in such basic parameters as the gain, the size of the working area and the threshold sensitivity.

In the 90s, Silicon Photoelectron Multipliers (SiPM) detectors, capable of detecting single photons at room temperature, were developed and are widely used. SiPM detectors operate in a higher breakdown voltage mode (or in Geiger mode) and have a wide range of photoresponse linearity by the number of photons in a pulse. Depending on the manufacturer, the SiPMs detectors are also called Micropixel Avalanche Photodiodes (MAPD) or Micro Pixel Photon Counters (MPPC). Currently, SiPM detectors in their main parameters, such as photon

detection efficiency, gain, photoresponse and working area, are significantly superior to SPAD and VLPC detectors. Therefore, the SiPM detector is considered the most adequate solid-state analogue of the PMT. Mass production of SiPM detectors has been achieved over the past decade. The main consumers of SiPM detectors are large-scale projects in high-energy physics, conducted at leading scientific centers, including the NICA project (Dubna, Russia). Tests are being conducted with the aim of mass using of SiPM detectors in the new generation of medical tomography and in the automotive industry (Lidar).

Structures of modern silicon photodiodes

There are two main types of photodiodes depending on the pixels location in the structure. There are SiPM with surface and deep buried pixel locations.

An example of the structure of a *photodiode with surface pixels* is presented in Figure 2.1.

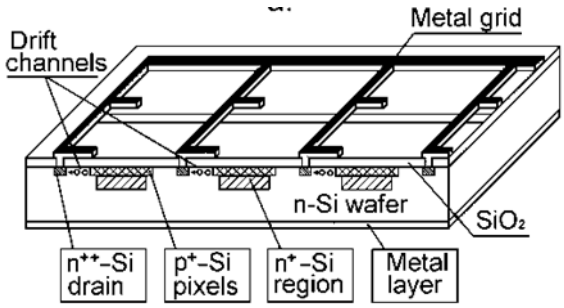

Figure 2.1. The section of the photodiode with the drift channel [13].

A negative voltage is applied to the gate connected to the drain, relative to the substrate, above the pixel breakdown voltage. In this case, a thin inverse p-type layer (drift channel) with high surface resistance is formed at the Si-SiO_2 interface. The resistance of this layer is used as a damping pixel resistance. The drift channel can be lightly doped with acceptor impurities to prevent oxide charging. After the end of the avalanche process, the pixel is charged through this conduction channel. SiPM with a surface pixel arrangement have a high charge multiplication factor (of

the order of 10^6, at the photomultiplier level), a good value of the photon detection coefficient (~15%) for photons in the visible region, a low value of the excess noise factor (close to unity) and others positive features. The combination of these qualities allows using this design to record weak light fluxes like single photons. Photodiodes with this design register less noise. Also for their work it is not necessary to apply too much voltage, as for a PMT. The signal received by this type of SiPM has a sharper rising edge. In addition, such photodiodes have a stable value of resistance, which has a positive effect on the recovery time.

Deep-hidden pixel photodiodes contain n-type silicon substrate, on the surface of which two epitaxial layers of p-type conductivity are grown. [14] (Fig.2.2).

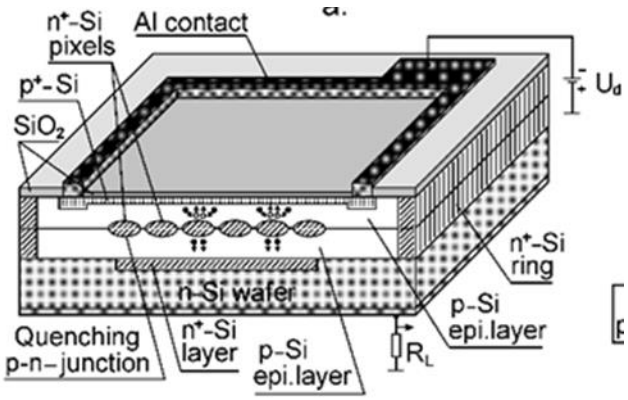

Figure 2.2. The section of SiPM with deep-hidden pixels [15].

A matrix of highly doped regions (pixels) of n + -type conductivity with a diameter of 2 ÷ 10 μm and with a step of 2 ÷ 5 μm is formed between the epitaxial layers [16]. In the operating mode, a negative voltage is applied to the photodiode relative to the substrate. Depletion of the device begins with the first p–n– junction located at the boundary of the substrate with the first epitaxial layer. At a certain voltage, the depleted region reaches the matrix of n + regions and partially opens the second p – n junction there. From this point, only the third p –n–junction, located on the boundary of the n+ regions with the second epitaxial layer, becomes depleted. A further increase of voltage leads to the complete depletion of the second epitaxial layer. As a result, a matrix of potential wells from n+ regions is formed in the depleted region of this type of SiPM, and a hemispherical electric

field is formed over each of these regions, which collects photoelectrons from the entire sensitive surface of the device.

One of the advantages of this type of photodiodes is that it can achieve a significantly higher pixel density than in other types (up to $4*10^4$ per mm2 with one hundred percent sensitivity of the entire area of the device) [15, 17]. The entire surface of this photodiode is 100% photosensitive, since there are no opaque zones on it that are not capable of creating an electron-hole pair. Thus, this makes it possible to increase the sensitivity of the device as a whole. Also, SiPM with deep-buried pixels are capable of detection even at low temperatures due to their special structure. In addition, photodiodes with a similar structure have a photodetection efficiency (PDE) twice as large as photodiodes with surface pixels (~ 40%).

The main parameters of silicon photodiodes

The work of SiPMs is characterized by the following parameters:

- Breakdown voltage and operating voltage;
- Dark current;
- Photodetection efficiency (PDE);
- Gain.

The *breakdown voltage* determines the point from which the detector starts working in Geiger mode.

There are several ways to determine the breakdown voltage:

1) The sharp increase in current in the reverse branch of the current-voltage characteristic when the detector goes into the Geiger mode of operation.

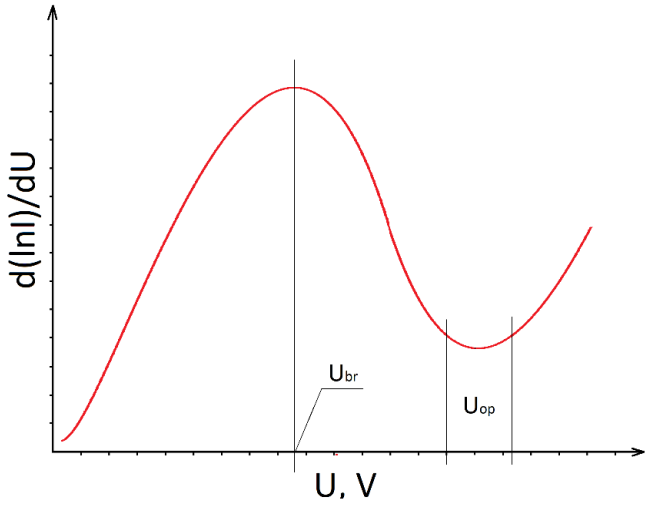

Figure 2.3. The curve of the function of the logarithmic derivative, where U_{br} is the breakdown voltage, U_{op} is the operating voltage interval.

2) According to the dependence of the reverse photocurrent on voltage.

3) When plotting the dependence of charge on a pixel on voltage and its approximation by a linear function. Then the point of intersection of this function with the abscissa axis (voltage) will give the value of the breakdown voltage.

The *operating voltage* is determined by the voltage interval in which the linearity of the gain is maintained and selected depending on the experimental conditions (Fig. 3).

Electron-hole pairs can also be formed in the absence of light flux due to such effects as:

1) thermogeneration;
2) tunneling of electrons from the valence band into the conduction band due to a high electric field.

Any free charger carrier, caught in the Geiger amplification zone, can cause the formation of an avalanche, the pulses at the output of SiPM will not differ from the photogenerated ones. Thus, the current generated due to the above effects will

be a noise signal. The term *dark current* is used to refer to this noise. It can be determined by any current meter (up to hundreds of picoamperes).

For SiPM, the *photodetection efficiency parameter* is defined as the ratio of the number of primary pixels to the number of incident photons at low light intensity:

$$\mathrm{PDE} = \frac{\mu}{N_{\mathrm{ph}}}. \quad (1)$$

The *gain* of SiPM is the ratio of the charge accumulated on the elementary capacity of the pixel during the development of the Geiger discharge to the electron charge:

$$\mathrm{M} = \frac{Q}{q}, \quad (2)$$

where q is the electron charge. The gain of SiPM shows how many times the photoelectron is multiplied as a result of the Geiger discharge.

Experimental results and discussions

In the present work, sixteen photodiodes were selected to create a 4x4 matrix. The main parameters of MAPD-3NM (photodiodes with a deep pixel arrangement) were investigated and those with the same parameters among the photodiodes were chosen.

Determination of breakdown voltage and operating voltage of MAPD-3NM

There are several ways to determine the breakdown voltage and operating voltage. In present work, the voltages were determined using the dark current differentiation method.

The experimental setup is schematically shown in figure 2.4, the installation photo is shown in figure 2.5.

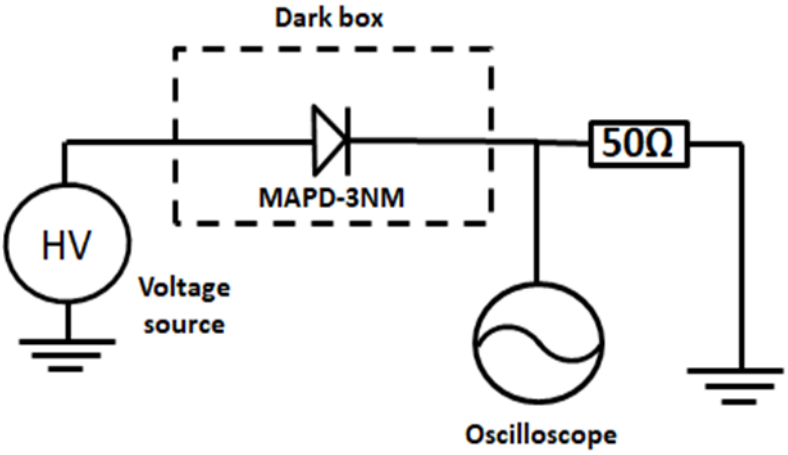

Figure 2.4. Experimental setup.

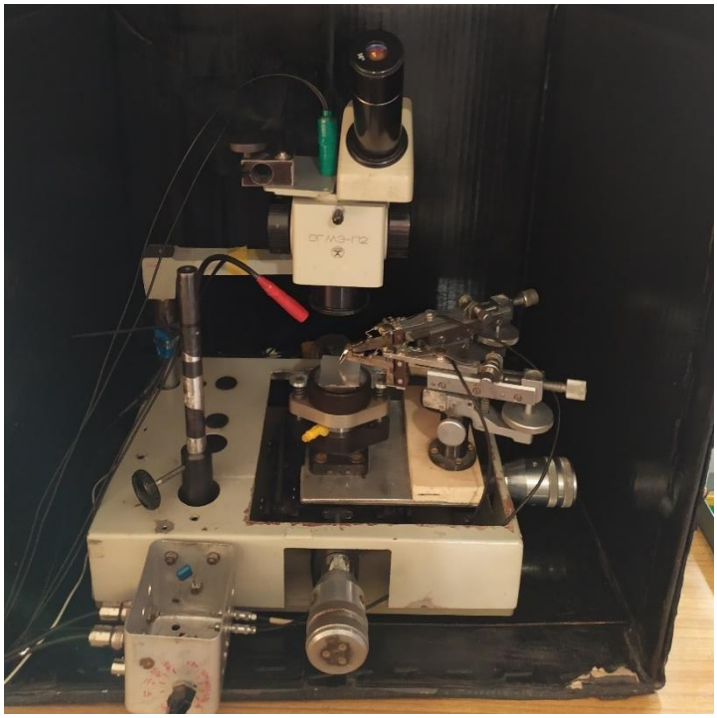

Figure 2.5. Photography of setup.

The samples were connected to a power source which was a KEITHLEY 6487 picoammeter. The entire setup was isolated from external light. Using a picoammeter, the values of the dark current I_d for a given voltage were found.

To determine the breakdown voltage and operating voltage, the current-voltage characteristics for each sample were taken, which were further analyzed. In this method, according to the obtained data, there was a maximum of the logarithmic derivative max[f(U)], where the function f(U) is found by the formula (3). The graph of the dependence f=f(U) is plotted.

$$f(U) = \frac{d(lnI(U))}{dU} = \frac{1}{I} \times \frac{dI(U)}{dU}. \quad (3)$$

By fitting the obtained curve, the Gauss function determines the point of the peak center, which corresponds to the breakdown voltage of the photodiode. The results of the measured I-V characteristics are shown in figure 2.6.

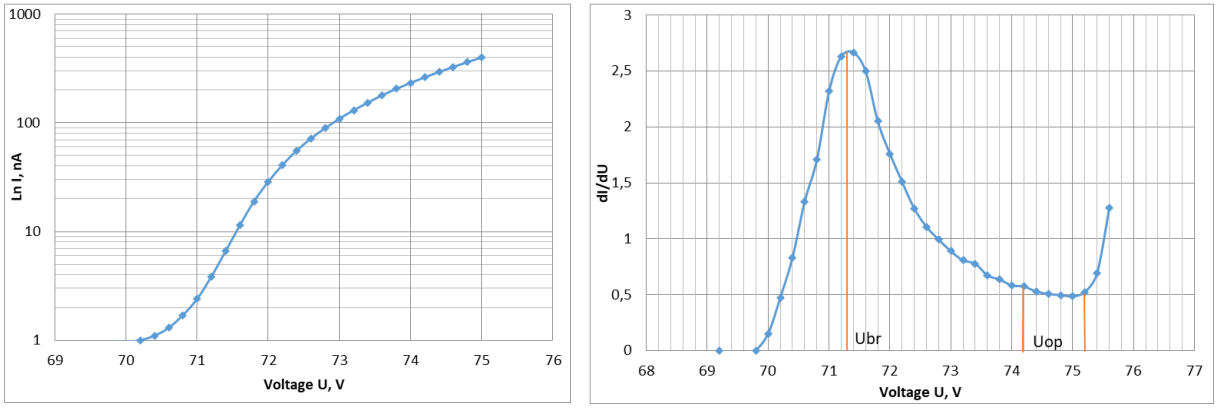

a) b)

Figure 2.6. I-V characteristics with logarithmic current scale (a) and I-V, obtained by differentiating the dark current (b).

According to this graph, it is possible to determine the values of breakdown voltages U_{br}, which were in the range 71 – 71.3 V, as well as operating voltages U_{op}, equal to 74.2 – 75.2 V. Measurements were carried out at a temperature of T ~ 21°C.

Determination of dark current of MAPD-3NM

The next step in the assembly of the matrix is the selection of certain photodiodes with the same parameters (dark current I_d, total current I_{tot}). A certain set of photodiodes is taken, in which subsequently the values of these parameters will be measured. This must be done because of the inhomogeneities created during the production of these diodes, which affect their characteristics. The setup required for the study of these characteristics is shown in figure 2.7.

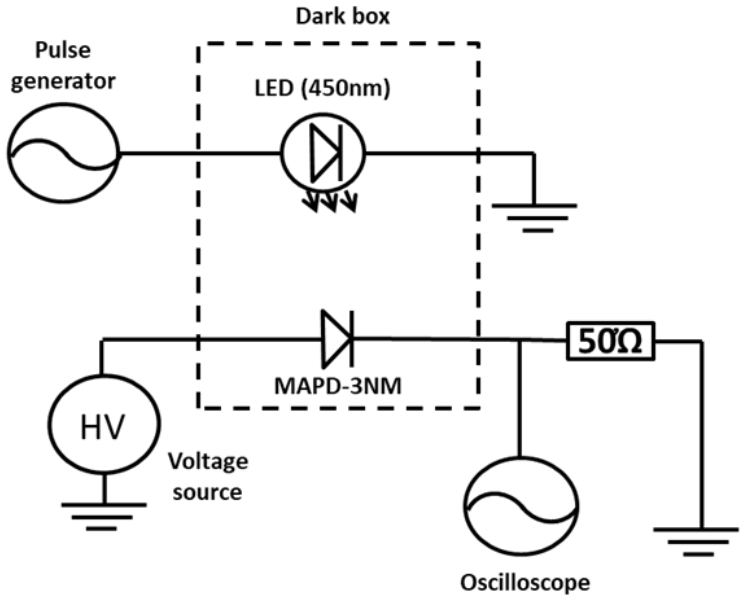

Figure 2.7. Experimental setup.

As for measuring the current-voltage characteristic, the photodiode is connected to a power source. The sample is illuminated by a light diode with a wavelength of 450 nm, which is supplied with a pulse length of 30 ns from the generator with a frequency of 1 kHz and an amplitude of 2.8 V. Picoammeter showed the value of the total current I_d.

At a certain voltage (~72.5 V), for which the signal amplitudes for different photodiodes were the same, the values of the currents I_d, I_{tot} were found. The voltage values for them could vary within 0.05 V. In total, the characteristics of forty different photodiodes were measured, in which the dark current ranged from 63 nA to 190 nA, and the total current ranged from 72 nA to 200 nA. Further, according to the results of the photodiode measurements, sixteen photodiodes were selected to create a 4x4 matrix. The selection of certain photodiodes was made by the similarity of parameters. After that, the selected MAPD photodiodes were attached to the textolite housing to the copper pads with conductive glue. Further the matrix covered with epoxy resin was placed in the furnace at a temperature of 60°C for full hardening of conductive glue and epoxy resin.

Determination of Photodetection Efficiency of MAPD-3NM

In addition to the characterization previously indicated, a PDE coefficient was determined. A reference sample of a Hamamatsu MPPC S13360-3025 photodiode, whose PDE is known (25%), was placed in the black box shown in Figure 2.8.

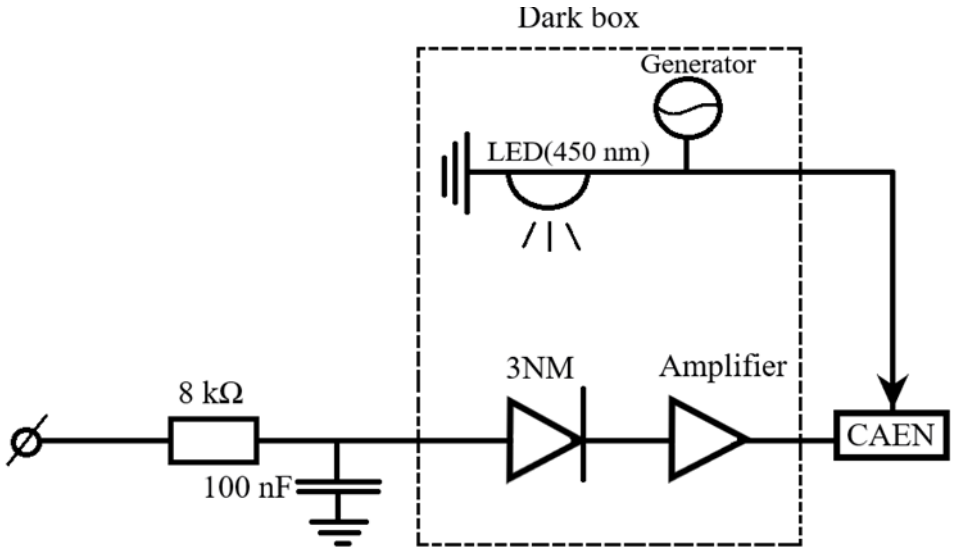

Figure 2.8. Experimental setup.

The sample was illuminated by a light diode with a wavelength of 450 nm, to which a 30 ns length pulse was supplied from a generator with a frequency of 50 kHz and an amplitude of 2.92 V. One of the methods indicated earlier was the breakdown voltage for a given temperature (in our case, the temperature was –6 ºC). It is known that for these photodiodes, the operating voltage is determined as follows:

$$U_{op} = U_{br}+5V. \quad (3)$$

At this temperature, U_{br} turned out to be equal to 50.08 V. By changing the voltage within five volts, we get the operating voltage. Using the single-photoelectron spectrum, the number of recorded events was determined and, using formula (4), the average number of registered photons in one pulse μ was found.

$$\mu = -\ln\left(\frac{N_{tot}-N_{det}}{N_{det}}\right), \quad (4)$$

where N_{tot} is the total number of events for these LED parameters that occurred in three minutes ($N_{tot} = F * t = 50 * 10^3 * 180 = 9 * 10^6$ counts), N_{det} is the number of registered events.

At an operating voltage of 55.08 V, the average number of registered photons in one pulse μ equal to $1.33*10^6$ was obtained. From formula (1) with a simple ratio we can find the number of photons, knowing the PDE for photodiodes Hamamatsu S13360-3025. It was found that their number is $5.3 * 10^6$. However, these photodiodes have an area of 3x3 mm, and MAPD-3NM, whose PDE will be measured later, have an area of 3.7x3.7 mm. From a simple relation it was found that for 3NM photodiodes the number of photons is $8.06 * 10^6$.

The reference photodiode was replaced by MAPD-3NM and cooled to the same temperature –6 ºC. Its breakdown voltage U_{br} = 71.2 V was determined, as well as the operating voltage in the manner described above. Further, for various operating voltages, the average number of registered photons in one pulse was found. The PDE was determined by the formula (1). The results of the studies are presented in table 1 below.

Table 1. PDE for different operating voltages for MAPD-3NM.

U, V	$\mu*10^6$, counts	PDE, %
73,7	2,16	26,7
74,2	2,25	27,9
74,7	2,4	29,8

Determining of the gain of MAPD-3NM

The gain measurement technique is similar to some steps in the PDE measurement technique. The test sample was placed in a black box, shown in Figure 8. It was cooled to a temperature of –3ºC.

Due to the fact that the signal passed through the CAEN analog-to-digital converter and amplifier, formula (2) undergoes some changes. The gain was

experimentally determined from the single-electron spectrum and calculated using formula (5):

$$M = \frac{X_c Y}{K_{amp} q}, \quad (5)$$

where Xc is the center of the first peak of the single-photoelectron spectrum, Y is the charge per channel (40 fC), K_{amp} is the amplifier gain, q is the electron charge.

For MAPD-3NM, the gain is $1.2 * 10^5$.

Conclusion

As a result of the studies, the structures and principles of operation of silicon photodiodes were studied. The main parameters characterizing SiPM were determined. As part of this work, the breakdown and operating voltages, dark current, gain, and PDE were determined for the MAPD-3NM. The value of the breakdown voltage U_{br} was equal to 71 – 71.3 V, the operating voltage U_{op} has values within 74.2 – 75.2 V. The dark current for these photodiodes varied in the range from 63 to 190 nA. The reference photodiode Hamamatsu S13360-3025 was used to determine the PDE of the test sample, which varies from 26-30% depending on the overvoltage value. The gain for MAPD-3NM was $1.2*10^5$.Based on the results of photodiode measurements, sixteen photodiodes with the same operating voltage were selected to create a 4x4 matrix. There is a table with the characteristics defined in this study for MAPD-3NM samples.

Table 2. Values of MAPD-3NM parameters.

Breakdown voltage U_{br}	71 – 71,6 V
Operating voltage U_{op}	74,2 – 75,2 V
Dark current I_d	63 nA – 190 nA
Photodetection efficiency	26-30%
Gain	$1,2*10^5$

The results of the practical work were published in the Polish journal Colloquium-journal, Sushkova P. M, Akbarov R. A, Nuruyev S. M, Tyutyunnikov S.I. “Assembling a matrix of photodiodes based on MAPD”, №16(40), part 5, pp 24.

Acknowledgement

I take this opportunity to express my profound gratitude and deep regards to my supervisor S. I. Tyutyunnikov for acquaintance with the various methods of spectrometry during my practice in Student Program of JINR that made my work here interesting and diverse.

I also take the opportunity to express a deep sense of gratitude to V. N. Shalyapin, R. A. Akbarov, A. Z. Sadigov, S. M Nuruyev for their valuable guidance which helped me completing my work through various stages.

Lastly, I would like to thank a committee of Summer Student Program for opportunity to visit Joint institute for nuclear research and for financial support.

References

1. Wang, C. T., et al. "Studies on the concentrations of arsenic, selenium, copper, zinc and iron in the hair of blackfoot disease patients in different clinical stages." Clinical Chemistry and Laboratory Medicine 32.3 (1994): 107-112.
2. Tsygankova, Alphiya R., et al. "Analysis of trace elements in the hair of farm animals by atomic emission spectrometry with Dc Arc excitation sources." Journal of Pharmaceutical Sciences and Research 9.5 (2017): 601.
3. Shalyapin, V. N., and S. I. Tyutyunnikov. "Design of the analyzer of the atomic composition of substances based on RF filamentary discharge." Physics of Particles and Nuclei Letters 12.5 (2015): 720-724.
4. Goullé, Jean-Pierre, et al. "Metal and metalloid multi-elementary ICP-MS validation in whole blood, plasma, urine and hair: Reference values." Forensic science international 153.1 (2005): 39-44.

5. McKay K. G. and McAfee K. B. “Electron multiplication in silicon and germanium”, Phys. Rev. 91(5) (1953) 1079–1084.
6. McKay K. G. “Avalanche breakdown in silicon”, Phys. Rev. 94(4) (1954) 877–884.
7. Wolff P. “Theory of electron multiplication in silicon and germanium”, Phys. Rev. 95(6) (1954) 1415–1420.
8. S. L. Miller. “Avalanche Breakdown in Germanium”, Phys. Rev., 99(4) (1955) 1234–1240.
9. L. V. Keldysh. “Influence of the lattice vibrations of a crystal on the production of electron-hole pairs in a strong electrical field”, Soviet Physics JETP 34(7) 4 (1958) 665–669.
10. L. V. Keldysh. “Kinetic theory of impact ionization in semiconductors”, Soviet Physics JETP 37(10) 3 (1960) 509–618.
11. Shockley W. “Problems related to p- n junctions in silicon. – Solid State Electronics”, 2(1) (1961) 35–60.
12. Baraff G. A. “Distribution Functions and Ionization Rates for Hot Electrons in Semiconductors”, Phys. Rev., 128(6) (1962) 2507–2517.
13. N. Anfimov, I. Chirikov-Zorin, Z. Krumshteyn, R. Leitner, A. Olchevski. “Test of micropixel avalanche photodiodes”, Nucl. Instr. and Meth. A572(1) (2007) 413–415.
14. Садыгов З.Я. Патент России № 2316848 2006 год.
15. N. Anfimov, I. Chirikov-Zorin,_, A. Dovlatov, O. Gavrishchuk, A. Guskov, N. Khovanskiy, Z. Krumshtein, R. Leitner, G. Meshcheryakov, A. Nagaytsev, A. Olchevski, T. Rezinko, A. Sadovskiy, Z. Sadygov, I. Savin, V. Tchalyshev, I. Tyapkin, G. Yarygin, F. Zerrouk. “Beam test of Shashlyk. EM calorimeter prototypes readout by novel MAPD with super high linearity”, Nucl. Instrum. Meth. A617(1-3) (2010) 78–80.
16. Z. Ya. Sadygov. “Microchannel avalanche photodiode”, Russian patent # 2316848, Application: 01.06.2006, date of publication: 10.02.2008.

17. N. Anfimov, I. Chirikov-Zorin, A. Dovlatov, O. Gavrishchuk, A. Guskov, N. Khovanskiy, Z. Krumshtein, R. Leitner , G. Meshcheryakov, A. Nagaytsev, A. Olchevski, T. Rezinko, A. Sadovskiy, Z. Sadygov, I. Savin, V. Tchalyshev, I. Tyapkin , G. Yarygin, F. Zerrouk. “Novel micropixel avalanche photodiodes (MAPD) with super high pixel density”, Nucl. Instrum. Meth. A628(1) (2011) 369–371.